Single-Mode Operation of a Bragg Free-Electron Maser Oscillator

T.S. Chu,* F.V. Hartemann,† B.G. Danly, and R.J. Temkin
Plasma Fusion Center, Massachusetts Institute of Technology, Cambridge, Massachusetts 02139
(Received 28 September 1993)

Detailed studies of the spectral characteristics and spatial mode structure of a single-mode, high-power Raman free-electron maser (FEM) oscillator operating with a Bragg resonator are reported. The FEM oscillator generated approximately 1 MW of microwave power in a single axial mode at 27.47 GHz, with an electron beam energy of 320 keV and a transmitted current of 30 A, yielding an efficiency of 10.3%, in good agreement with nonlinear simulations. These results indicate that a Raman free-electron maser can operate at high power and efficiency with stable single-mode output in the long pulse (equilibrium) regime.

PACS numbers: 41.60.Cr, 52.75.Ms

Free-electron lasers (FELs) or masers (FEMs), as they should be termed for the microwave region of the spectrum, are tunable sources of intense coherent electromagnetic radiation [1,2]. Some of their most remarkable properties include tunability [3], wide bandwidth [4], high gain [5], and the large phase shift that the resonant beam-wave interaction induces on the amplified electromagnetic wave [6]. Potential applications of FEM amplifiers and oscillators are numerous, and include their use for radar and plasma heating. Operation of the FEM oscillators in a single mode at high efficiency is of paramount importance for these applications; thus the avoidance of mode competition effects, which are known to be prevalent in FEM and FEL oscillators [7], becomes a primary concern. This paper reports on the successful single-mode operation of a high-power FEM oscillator. Mode competition results are discussed in the context of multimode oscillator theory [7] and previous experiments [8].

Several past experiments on FEM oscillators have been reported. Pioneering work at Columbia [9] and NRL [10] showed the possibility of generating high power microwave oscillations by providing feedback to the growing electromagnetic waves amplified by the FEL interaction. More recently, FEM oscillators employing Bragg resonators have been described [11,12]. The work at Hughes [11] is especially relevant as it demonstrated stable, long-pulse, moderate power operation of a Bragg FEM oscillator in the Compton regime. Other experiments [12] were in the Raman regime, but at short pulse and wide bandwidth. In contrast to earlier long-pulse experiments [11], the present experiments [13] are in the Raman regime and at high power, and, in addition, a careful study of the spectral properties of the FEM radiation has been carried out. In particular, the detailed spatial (transverse and axial) and temporal (mode competition) [7] structure of the operating mode has been studied experimentally. In the present experiment, the axial modes of the Bragg resonator have been clearly identified, and very good agreement between the theoretically predicted efficiency and the experimentally measured output power has been shown. Most previous experiments with free-electron masers operating in the Raman regime have operated with short pulses. Those experiments have either run with pulses of 10 to 100 ns duration or have had large ($> 5\%$) voltage and current variations on that time scale. The present experiments have operated with flat ($< 0.25\%$ ripple) voltage and current pulses in the microsecond regime, which is long compared with the cavity equilibrium time for both growth of modes and mode competition. As described below, the long pulses of the present experiment provide a critical test of the mode competition effects in a highly overmoded cavity. Such a test is important if the FEM is to find practical applications.

The evolution of the mode spectrum in optical FELs is generally characterized by the slippage parameter, ϵ, which is a measure of the difference between the wave group velocity and the beam velocity. The slippage is defined by $\epsilon = (L/L_c)(v_g/v_\parallel - 1)$, where L and L_c are the length of the gain section and the length of the cavity, respectively, and where v_g and $v_\parallel$ are the wave group velocity and the beam parallel velocity, respectively [7]. For optical FELs, the time required for the cavity fields to reach equilibrium is of order $\tau \sim Q/\omega\epsilon^2$. This time may be quite long compared to the beam pulse lengths found in most FEL experiments [8], because the slippage is generally quite small.

In contrast to the case of optical FELs, for millimeter wave FEMs operating with waveguide resonators, the slippage may be quite large. Consequently, one may expect a rapid evolution of the mode spectrum of the resonator into a final stable state. Moreover, in addition to this enhanced communication between different segments of the radiation pulse due to the larger slippage, the addition of dispersion in the resonator is known to significantly shorten the time required to reach an equilibrium state [14]. The distributed nature of the feedback provided by the Bragg reflectors which constitute the end reflectors for the Bragg resonator result in highly dispersive reflection and a cavity which is highly frequency selective. This special property of the Bragg resonator

0031-9007/94/72(15)/2391(4)$06.00

modifies the physics of mode competition in the FEM oscillator because the dispersive effects induced by the resonator now dominate over slippage, which has been identified as the main mode-selection mechanism in low gain Compton FEL oscillators operating with optical cavities [7,8,14].

In this experiment, depicted in Fig. 1, the Bragg resonator consists of a straight section of circular waveguide together with two end reflectors which provide feedback in the transverse circular TE_{11} mode at frequencies ($\omega/2\pi \simeq 27.4\,\mathrm{GHz}$) considerably higher than the cutoff frequency ($\omega_c/2\pi \simeq 11\,\mathrm{GHz}$). The corrugated sections provide feedback by coupling forward propagating waves (f^+, k^+) to backward propagating waves (f^-, k^-), where $f^\pm$ are the respective slowly varying complex amplitudes of the waves, and $k^\pm$ are the axial components of the respective wave vectors. The coupling occurs when the wave number matching (Bragg) condition, $|k^+| + |k^-| = k_B$, is satisfied. Here, $k_B = 2\pi/\lambda_B$ and $\lambda_B = 5.84\,\mathrm{mm}$ is the wavelength of the corrugations in the reflector. For small amplitude corrugations, Bragg reflectors and resonators may be modeled by coupled mode theory [15,16].

The eigenmodes of a Bragg resonator may be obtained by solution of the coupled mode equations for the field amplitudes $f^+(z)$ and $f^-(z)$ subject to appropriate boundary conditions. Solution of the eigenvalue problem for complex frequency ω yields both the eigenvalues $\omega = \omega_r + i\omega_i$ and thereby the diffractive Q, $Q_D = \omega_r/2\omega_i$, as well as the eigenfunctions f^+ and f^- for the cold-cavity fields in the resonator. The field profiles determined in this manner may then be used to calculate the energy transfer from the beam to the wave in nonlinear simulations. The solution for the complex eigenfunctions f^+ and f^- for the primary mode at 27.4 GHz are shown in Fig. 2. The solution for $|f^+ + f^-|^2$ is shown, together with $|f^+|^2$ and $|f^-|^2$, which are proportional to the traveling-wave power in the forward and backward directions, respectively. The diffractive Q for the primary mode of the Bragg resonator employed in this experiment is $Q = 453$. Three other axial modes, which also have TE_{11} transverse structure, are also present in the theoretical spectrum of the resonator: modes at 27.1, 28.1, and 28.3 GHz. For the three lower frequency modes observed in the experiment, all three had starting currents lower than the beam current at the nominal operating beam energy of 310–320 keV. For this reason, mode competition is a significant issue for the present experiment.

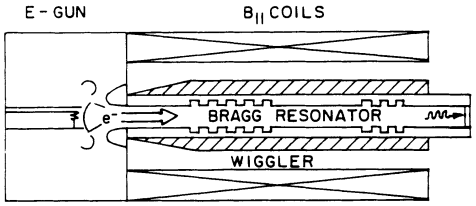

FIG. 1. Overall experimental setup and schematic of the Bragg resonator.

The overall experimental setup is illustrated by Fig. 1. Apart from the Bragg resonator, the other main components of the device are the high-voltage modulator, the thermionic electron gun, the solenoids which produce the axial magnetic field, and the helical permanent magnet wiggler. The system operates with a flattop pulse length $\tau = 1\,\mu\mathrm{s}$. Beam compression to a radius of 4 mm was achieved with minimal (< 5%) scalloping, in good agreement with adiabatic theory. The beam axial energy spread, before injection into the wiggler interaction region, is inferred from experimental data to be $\Delta\gamma_{||}/\gamma_{||} < 0.5\%$. The beam is transported through the interaction region by an axial magnetic field of magnitude 2.35 kG. A permanent magnet helical wiggler with 3 cm period and 500 G amplitude is used to provide the perpendicular momentum of the interacting electrons. To ensure stable high-quality group I helical orbits in the interaction region, the wiggler has a 10-period long linearly tapered introduction. The resulting equilibrium orbits at 320 keV beam energy have theoretically calculated $\beta_\perp = 0.18$, $\beta_{||} = 0.76$, and a wiggler parameter $\Phi = 1.1$ [17]. The Bragg resonator is entirely located in the constant amplitude wiggler region. The large reflectivity Bragg reflector (on the gun side) has $N_1 = 68$ periods, and the outcoupling reflector has $N_2 = 22$ periods. The cavity itself, between the corrugated sections, is very compact with a length of 10 cm. The mean radius of the reflectors and cavity is 8.3 mm. The output microwave circuit is composed of a TE_{11} directional coupler and a well-matched (reflection < 0.25%) load.

The operating point yielding the high power output of $P^+_{\mu w} = 990\,\mathrm{kW}$ was obtained for the following parameters: beam voltage $V = 320$ kV, injected current $I_b = 49$ A, transmitted current $I_t = 30$ A. The loss of current in the transport is believed to be due to two effects: (1) transverse field errors in the solenoidal focusing magnets, and (2) the relative proximity of the FEL cyclotron resonance. Such losses are believed to occur in the transport system upstream of the Bragg resonator because the beam propagated through the wiggler uptaper and through several regions of solenoid field error before en-

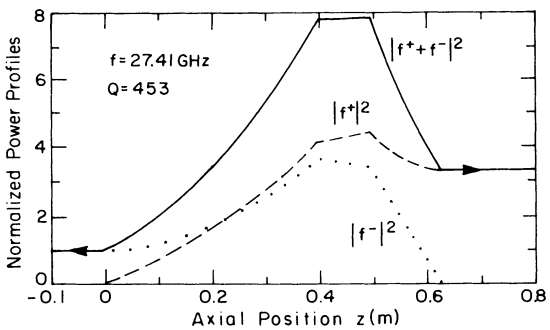

FIG. 2. Bragg resonator eigenmode profiles.

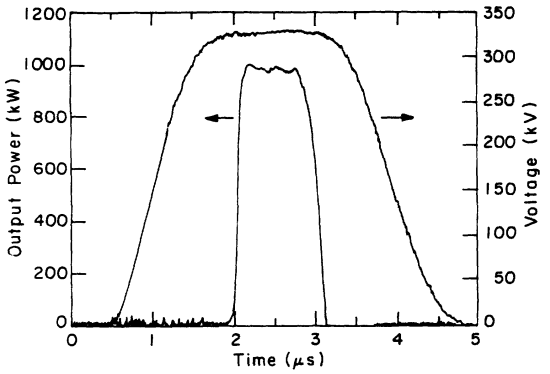

FIG. 3. Microwave power (diode signal) and voltage wave forms.

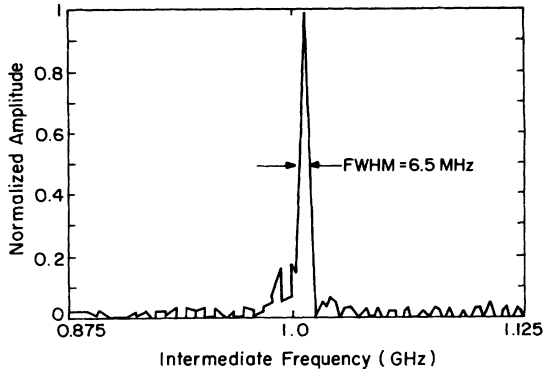

FIG. 4. Measured IF spectrum of FEM output, showing single-mode operation.

tering the Bragg resonator.

For the electron beam parameters given above, the system operates in a single mode at a frequency $\omega/2\pi = 27.47\,\mathrm{GHz}$, with a linewidth $\delta\omega/2\pi < 10\,\mathrm{MHz}$. The diode signal corresponding to the power measurement, and the corresponding beam voltage wave form are shown in Fig. 3. The overall experimental uncertainty on the output power level is ± 0.5 dB. These measurements were confirmed by calorimetry. The corresponding electronic efficiency, defined as $\eta = P^{+}_{\mu w}/VI_t$, is $\eta = 10.3\%$. Measurement of the far-field radiation pattern confirmed operation in the TE_{11} mode.

The frequency of the FEM output power was measured by mixing the output signal with a tunable local oscillator and then sampling and Fourier transforming the resulting intermediate frequency (IF) with a 2 gigasample per second digital storage oscilliscope. This technique allowed identification of the mode of oscillation of the cavity. The IF spectrum for the main operating mode at 27.4 GHz is shown in Fig. 4.

The oscillator starting current was also measured; reduction of the cathode temperature decreased the beam current in the FEM interaction region and permitted a measurement of the starting current. The starting current for the mode considered here is measured to be $I_s = 4$ A. A peak efficiency of 12.5% was also achieved for a transmitted current $I_t = 23\,\mathrm{A}$, at a power level of $P^{+}_{\mu w} = 920\,\mathrm{kW}$.

Single-mode operation of the FEM on two additional axial modes of the Bragg resonator was also obtained at frequencies of 27.1 and 28.1 GHz, by tuning of the electron beam energy. The primary mode at 27.4 GHz was excited for beam energies from 308 to 323 keV, the 27.1 GHz mode was excited for beam energies from 297 to 306 keV, and the 28.1 GHz mode was excited for energies from 330 to 340 keV. For each of these energy ranges, the FEM operated in a single mode. For beam energies in the narrow range from 306 to 308 keV and 323 to 330 keV, low-power multimode operation was present. The experimentally observed oscillation frequencies correspond very closely to the theoretically calculated frequencies of the Bragg resonator eigenmodes. A systematic frequency shift of $\Delta\omega/2\pi = 70\,\mathrm{MHz}$ as compared with the calculated resonant frequency is observed. Whether this is due to a nonlinear frequency pulling or due to cavity machining errors cannot be determined with certainty. The tolerance on the Bragg period was $\pm 0.9\%$, which could produce a shift of the Bragg eigenmode frequency by up to 250 MHz if the error were systematic. The cold tests of the resonator agreed with the calculated eigenmode frequencies to within the error of the cold test, which was $\sim \pm\omega/2\pi Q = 60\,\mathrm{MHz}$.

The nonlinear Raman FEL amplifier code RAMFEL [18] has been modified to model the present results. This code is a one-dimensional single-mode code which takes into account the longitudinal space-charge waves. It couples single particles describing helical trajectories under the combined effects of the wiggler and guide magnetic fields to the slowly varying amplitude and phase of the TE_{11} cylindrical waveguide mode. To model steady-state operation of a Bragg oscillator, the field equations are replaced by a fixed field profile corresponding to the eigenmode calculated from the coupled-mode theory analysis of the Bragg resonator. The axial variation of the field is

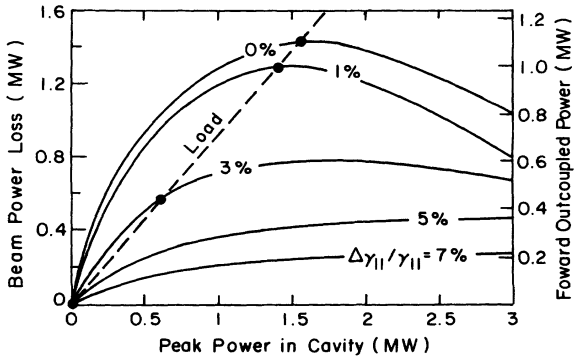

FIG. 5. Comparison of nonlinear oscillator simulations with experiment. The experimentally measured forward outcoupled power of 990 kW is seen to agree well with the simulation for a spread of $\Delta\gamma_{\parallel}/\gamma_{\parallel} = 1\%$.

prescribed by the eigenmode; however, the amplitude of the field in the cavity is determined self-consistently by power balance. The results of this analysis are presented in Fig. 5 for a beam of 30 A and 320 keV. In Fig. 5, the solid curves represent the calculated beam power loss as a function of the peak traveling-wave power in the cavity [$\hat{P}^+ \propto |f^+(z = 0.5\,\mathrm{m})|^2$] for different spreads. The load line, which has a slope of $\omega W/Q\,\hat{P}^+ = 0.91$ where W is the stored energy, is also shown. The stable operating point for the cavity is determined by satisfying energy conservation:

$$I_t\,(m_0c^2/e)\langle\gamma_{\mathrm{in}} - \gamma_{\mathrm{out}}\rangle = P^+_{\mu w} + P^-_{\mu w}, \qquad (1)$$

where $\langle\gamma_{\mathrm{in}} - \gamma_{\mathrm{out}}\rangle$ is the normalized average electron energy loss in the cavity, I_t is the beam current propagating through the cavity, and $P^+_{\mu w}$ and $P^-_{\mu w}$ are the forward and backward outcoupled powers, respectively. The right vertical axis is related to the left vertical axis by the fraction of forward outcoupled power to the total outcoupled power, which can be seen from Fig. 2 to be 0.77. The stable operating points of the oscillator are determined for different values of the beam axial energy spread in the wiggler. We see that for very large spreads ($\gtrsim 5\%$) there is no operating point, which indicates that the beam current is smaller than the corresponding starting current.

The observed experimental efficiency indicates that the effective energy spread in the wiggler is $\Delta\gamma_{\|}/\gamma_{\|} \simeq 1\%$. This spread results from a combination of wiggler field errors, guide field errors, beam emittance, and space-charge effects; this spread is consistent with computer trajectory simulations. We also note that the Q of the resonator is properly matched to optimize the total output power for the load line shown. However, there is a significant loss of power out the back of the Bragg resonator, thus lowering the operational efficiency as defined by the ratio of forward coupled power to beam power.

In conclusion, we have designed and operated a stable Raman free-electron maser oscillator with a Bragg resonator. The FEM oscillator generated 990 kW (±0.5 dB) of microwave power in a single axial mode at 27.4 GHz with a beam voltage of 320 kV and a transmitted current of 30 A, yielding an efficiency of 10.3%, in good agreement with nonlinear simulations. The microwave power pulse had a length equal to that of the transmitted current pulse, thus indicating the possibility of scaling the device for long-pulse operation. The starting current of this mode was measured to be 4 A, and a peak efficiency of 12.5% was observed for $I_t = 23$ A and $P_{\mu w} = 920$ kW. The system was operated with three of the four axial modes of the Bragg resonator.

We do not observe any competition between these axial modes over the range of voltages for which each is strongly excited. Each axial mode can be excited separately by varying the electron beam energy. This result suggests that the highly dispersive and frequency-selective nature of the feedback provided by the Bragg structure strongly modifies the physics of mode competition in the FEM oscillator. The slippage parameter for the present experiment is $\epsilon = 0.16$, corresponding to a characteristic time to equilibrium of $\tau \sim Q/\omega\epsilon^2 \sim 100$ ns for the primary mode at 27.4 GHz. In addition, it is anticipated that the dispersive effects induced by the Bragg resonator reduce this time even further, in a manner analogous to that demonstrated theoretically for a conventional optical resonator in [14].

This work was supported by Thomson Tubes Electroniques and the U.S. Department of Energy Contract No. DE-FG02-89ER14052.

* Present address: Varian Associates, Bldg. 2, M/S B118, 811 Hansen Way, Palo Alto, CA 94303.
† Present address: Electrical Engineering Department, University of California, Davis, Davis, CA 95616.

[1] T. C. Marshall, *Free Electron Lasers* (Macmillan Publishing Company, New York, 1985).
[2] C.W. Roberson and P. Sprangle, Phys. Fluids B **1**, 3–42 (1989).
[3] J. Fajans, G. Bekefi, Y.Z. Yin, and B. Lax, Phys. Fluids **28**, 1995 (1985).
[4] D.E. Pershing, R.H. Jackson, H. Bluem, and H.P. Freund, Nucl. Instrum. Methods Phys. Res., Sect. A **296**, 199–204 (1990).
[5] T.J. Orzechowski, B.R. Anderson, J.C. Clark, W.M. Fawley, A.C. Paul, D. Prosnitz, E.T. Scharlemann, and S.M. Yarema, Phys. Rev. Lett. **58**, 2172–2175 (1986).
[6] F. Hartemann, K. Xu, G. Bekefi, J.S. Wurtele, and J. Fajans, Phys. Rev. Lett. **59**, 1177 (1987).
[7] T.M. Antonsen, Jr. and B. Levush, Phys. Rev. Lett. **62**, 1488–1491 (1989).
[8] B.G. Danly, S.G. Evangelides, T.S. Chu, R.J. Temkin, G. Ramian, and J. Hu, Phys. Rev. Lett. **65**, 2251–2254 (1990).
[9] D.B. McDermott, T.C. Marshall, R.K. Parker, and V.L. Granatstein, Phys. Rev. Lett. **41**, 1368 (1978).
[10] J. Mathew and J.A. Pasour, Phys. Rev. Lett. **56**, 1805 (1986).
[11] R.J. Harvey and F.A. Dolezal, Appl. Phys. Lett. **53**, 1150 (1988).
[12] J. Chen, M.C. Wang, Z. Wang, Z. Lu, L. Zhang, and B. Feng, IEEE J. Quantum Electron. **27**, 488–495 (1991).
[13] B.G. Danly, F.V. Hartemann, T.S. Chu, P. Legorburu, W.L. Menninger, R.J. Temkin, G. Faillon, and G. Mourier, Phys. Fluids B **4**, 2307–2314 (1992).
[14] E.R. Stanford and T.M. Antonsen, Jr., Nucl. Instrum. Methods Phys. Res., Sect. A **304**, 659–662 (1991).
[15] G.G. Denisov and M.G. Reznikov, Radiophys. Quantum Electron. **25**, 407–413 (1982).
[16] M.C. Wang, V.L. Granatstein, and R.A. Kehs, Appl. Phys. Lett. **48**, 817 (1986).
[17] H.P. Freund and A.K. Ganguly, IEEE J. Quantum Electron. **21**, 1073 (1985).
[18] J.S. Wurtele, R. Chu, and J. Fajans, Phys. Fluids B **2**, 1626–1634 (1990).